Biophysical Reviews (2022) 14:1369–1378
https://doi.org/10.1007/s12551-022-01034-5

REVIEW

Quantum chemical studies on hydrogen bonds in helical secondary structures

Yu Takano[1,2] · Hiroko X. Kondo[1,3,4] · Haruki Nakamura[2]

Received: 30 September 2022 / Accepted: 30 November 2022 / Published online: 6 January 2023

Abstract

We present a brief review of our recent computational studies of hydrogen bonds (H-bonds) in helical secondary structures of proteins, α-helix and 3_{10}-helix, using a Negative Fragmentation Approach with density functional theory. We found that the depolarized electronic structures of the carbonyl oxygen of the *i*th residue and the amide hydrogen of the $(i+4)$th residue cause weaker H-bond in an α-helix than in an isolated H-bond. Our calculations showed that the H-bond energies in the 3_{10}-helix were also weaker than those of the isolated H-bonds. In the 3_{10}-helices, the adjacent N–H group at the $(i+1)$th residue was closer to the C=O group of the H-bond pair than the adjacent C=O group in the 3_{10}-helices, whereas the adjacent C=O group at the $(i+1)$th residue was close to the H-bond acceptor in α-helices. Therefore, the destabilization of the H-bond is attributed to the depolarization caused by the adjacent residue of the helical backbone connecting the H-bond donor and acceptor. The differences in the change in electron density revealed that such depolarizations were caused by the local electronic interactions in their neighborhood inside the helical structure and redistributed the electron density. We also present the improvements in the force field of classical molecular simulation, based on our findings.

Keywords Hydrogen bond · Secondary structure · Density functional theory · Negative fragment approach · α-Helix · 3_{10}-Helix

Introduction

Proteins are found in all living organisms and are involved in almost all biological activities such as catalysis, molecular recognition, and material transport (Liljas et al. 2017; Branden and Tooze 2012). Since protein functions are strongly correlated with their three-dimensional structures, understanding the three-dimensional structure of proteins and their dynamic behaviors is essential for various scientific fields including chemistry, biology, medicine, agriculture, and food industry.

Proteins are biopolymers consisting of a large number of amino acids held together by peptide bonds. Protein structures are hierarchical, with distinct levels of structures (Holde Van et al. 1998), which represent increasing levels of complexity and include primary, secondary, tertiary, and quaternary structures. Secondary structure is the local and regular structure of a protein, including α- and 3_{10}-helices, β-strands, and β- and γ-turns. These secondary structures are properly assembled to form tertiary structures. Thus, secondary structures can be considered the building elements of protein structures.

In secondary structures, a helix (e.g., α-helix and 3_{10}-helix) is a group of residues that repeatedly rotate and rise along an axis. It is the most observed secondary structure. We can classify it into different helical conformations. The α-helix is found in 31% of all secondary structures and is the most widely recognized helical structural element in fibrous and globular proteins (Barlow and Thornton 1988).

✉ Yu Takano
ytakano@hiroshima-cu.ac.jp

1 Graduate School of Information Sciences, Hiroshima City University, Hiroshima 731-3194, Japan

2 Institute for Protein Research, Osaka University, Suita 565-0871, Japan

3 Faculty of Engineering, Kitami Institute of Technology, Kitami 090-8507, Japan

4 RIKEN Center for Biosystems Dynamics Research, Suita 565-0874, Japan

The second most common helical structure is the 3_{10}-helix, which occupies 4% of the secondary structures.

These helices are stabilized by hydrogen bonds (H-bonds) formed between the amide hydrogens (the H-bond donors) and the carbonyl oxygens (the H-bond acceptors) of peptide bonds. H-bonds are one of the most important noncovalent interactions for chemical and biological phenomena (Saleh et al. 2012; Tantardini 2019; Tantardini et al. 2020). The significance of H-bonds in the secondary structures of proteins was recognized early (Pauling et al. 1951; Eisenberg 2003). The α-helix has 3.6 residues per turn and is a right-handed helix. In the α-helix, a H-bond is formed between the peptide carbonyl group at residue *i* and the peptide amino group at residue $i+4$. In contrast, the 3_{10}-helix has three residues per turn and is a right-handed helix. It has a H-bond between the peptide carbonyl group at residue *i* and the peptide amino group at residue $i+3$, resulting in a tighter packing of the backbone compared with the α-helix (Fig. S1). Many computational chemists have studied H-bonds in secondary structures at various levels of theoretical depth. Wieczorek and Dannenberg (2003a, b) investigated H-bond cooperativity and the energetics of α-helices, suggesting that various factors contribute to their stability. Morozov et al. (2006) evaluated the origin of cooperativity in forming α-helices. Wu and Zhao (2001) studied the role of cooperativity in the formation of α-helices by performing theoretical calculations on α-helix models constructed using a simple repeating unit method. Parthasarathi et al. (2007) studied H-bond interactions in an α-helix model using the atom-in-molecules method. Ismer et al. (2008) investigated the temperature dependence of the stability of α-, π-, and 3_{10}-helices compared with a fully extended structure using density functional theory (DFT) and harmonic approximation. However, a simple physicochemical theory accounting for helical secondary structural features of proteins is still immature.

An accurate and quantitative evaluation of H-bonds is also important for molecular dynamics (MD) simulations to investigate the dynamical behavior and folding process of proteins. Historically, it has been noticed since many years ago that each force field used in classical MD simulations shows a specific tendency to form an α-helix or a β-strand. For example, the AMBER C96 force field, which was developed just after the original AMBER force field (Cornell et al. 1995), preferred extended structures contrast to the α-helical preference of the latter one as mentioned by Kollman et al. (1997). This phenomenon has been repeatedly reported by many authors (Sakae and Okamoto 2003; Yoda et al. 2004a, b; Best et al. 2008; Best and Hummer 2009; Piana et al. 2011). Usually, this preference for force fields on the secondary structure formation is not a significant problem in the MD simulations of rigid globular protein structures. However, it has become a critical issue in understanding functionally important conformational changes (Higo et al. 2011; Shirai et al. 2014; Chebaro et al. 2015; Nishigami et al. 2016) in the folding simulations of flexible disordered regions (Higo et al. 2011; Chebaro et al. 2015) and long loops between secondary structures (Shirai et al. 2014; Nishigami et al. 2016). Yoda et al. (2004a, b) performed MD simulations to compare the secondary structural properties of commonly used force fields, finding that MD simulations with the AMBER ff94 (Cornell et al. 1995) and ff99 (Wang et al. 2000) force fields were in remarkable agreement with experimental data for α-helical polypeptides but not for β-hairpin polypeptides. Numerous attempts have been made to overcome this problem, such as increasing the torsional energies, rearrangements (Kamiya et al. 2005; Buck et al. 2006; Fujitani et al. 2009; Robustelli et al. 2018), and developing polarized charge models (Patel and Brooks 2004; Lopes et al. 2009). Regardless, the reasons behind the use of these methods remain unclear, and elucidation requires understanding the energy of hydrogen bonding in the secondary structure.

Here, we briefly review our computational studies of H-bonds in helical secondary structures of proteins, α-helix and 3_{10}-helix, using a Negative Fragmentation Approach (NFA) with DFT (Kondo et al. 2019, 2022). We will also discuss the modification of the force field, approximating the H-bond energies, revealed by our findings.

Model constructions and computational method

Model constructions

We constructed whole-helix (WH) models of an α-helix and a 3_{10}-helix, denoted as WH_{alpha}-*n* and WH_{3_10}-*n* models, respectively. In the model construction, we used poly-alanine amino acids capped with an acetyl group (ACE) and an *N*-methyl amide group (NME), denoted as ACE–$(Ala)_n$–NME ($n = 2$–7 for the 3_{10}-helices and $n = 3$–8 for the α-helices). The backbone torsion angles, φ and ψ, of the WH_{alpha}-*n* and WH_{3_10}-*n* models were set to their ideal values, as described in biochemistry textbooks, namely, $\varphi = -57°$ and $\psi = -47°$ for the WH_{alpha}-*n* models and $\varphi = -49°$ and $\psi = -26°$ for the WH_{3_10}-*n* models (Arnott and Dover 1967; Petsko and Ringe 2004; Kuster et al. 2015). These structures were optimized in the gas phase by fixing the backbone dihedral angles at the aforementioned values and minimizing the total electronic energies. One to six backbone H-bonds exist in the optimized WH_{alpha}-*n* and WH_{3_10}-*n* models. The *s*th H-bond in these models, counting from the *N*-terminus, is represented by *n*-*s*.

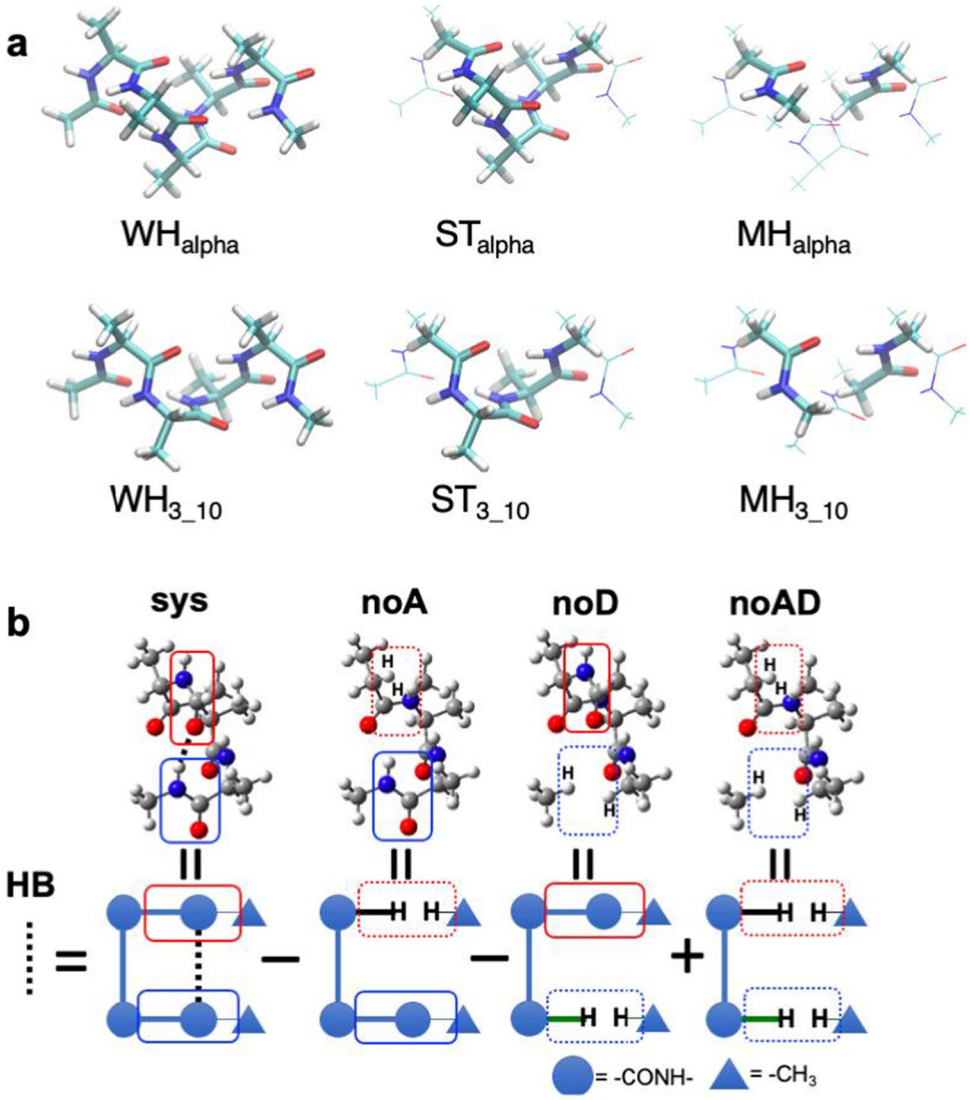

Fig. 1 **a** Structures of the WH_{alpha}-5, ST_{alpha}-5, and MH_{alpha}-5 models for an α-helix and those of the WH_{3_10}-4, ST_{3_10}-4, and MH_{3_10}-4 models for a 3_{10}-helix as examples. **b** Fragment structures and schematic picture for calculations of H-bond energy of 3–1 of the WH_{alpha}-3 model with NFA

To understand the characteristics of the H-bond energies in α-helices and 3_{10}-helices, we constructed two types of simplified models. One is a single-turn (ST) model, denoted as the ST_{alpha}-*n* and ST_{3_10}-*n* model composed of ACE-$(Ala)_3$-NME and ACE-$(Ala)_2$-NME, respectively. In this model, the H-bond donor and acceptor are linked with the helical backbone atoms. The other is a minimal H-bond (MH) model, denoted as MH_{alpha}-*n* and MH_{3_10}-*n* models comprising two separated *N*-methyl acetamide molecules and mimicking a single H-bond between the C=O and N–H groups in the backbone. In the MH_{alpha}-*n* and MH_{3_10}-*n* models, the two peptide groups forming a H-bond, hydrogen donors and acceptors, were separated without linking the helical backbone atoms. The atomic positions of these simplified models were the same as those of the corresponding WH_{alpha} and WH_{3_10} models, except for the N- and C-terminal capping groups. Figure 1a shows the molecular structures of the WH_{alpha}-5, ST_{alpha}-5, and MH_{alpha}-5 models for an α-helix and those of the WH_{3_10}-4, ST_{3_10}-4, and MH_{3_10}-4 models for a 3_{10}-helix as examples. The individual H-bond energy for these models was calculated in the same manner as that for each backbone H-bond in the WH models, as described below. The H-bond energies of these models were then compared to each other.

Validity of DFT exchange–correlation functionals for the calculation of H-bond energy of secondary structure

In recent years, DFT has become accepted as an alternative approach for the post Hartree–Fock (HF) methods such as Møller–Plesset perturbation theory (Head-Gordon et al. 1988) and coupled cluster theory (Scuseria and Schaefer 1989). In previous studies (Takano et al. 2011, 2012), we showed the importance of assessing the validity of

various DFT exchange–correlation functionals. The DFT exchange–correlation functionals was also validated for the H-bond energies of the ACE-$(Ala)_n$-NME system. We chose the B97D (B97 functional with Grimme's D2 dispersion schemes) exchange–correlation functional (Grimme 2006) with 6–31+G(d) basis sets because it provided the H-bond energies of an ACE–$(Ala)_n$-NME dimer comparable with the MP2 method in the calculation of the H-bond interaction energies of the ACE–$(Ala)_n$-NME system in the gas phase (Takano et al. 2016). This method was applied to H-bond energy calculations of the helical secondary structures composed of ACE–$(Ala)_n$-NME.

Negative fragmentation approach

Since it is not straightforward to calculate a H-bond energy of a molecule, where the donor and acceptor atoms are linked through covalent bonds, we utilized the NFA, which is the modified version of the Molecular Tailoring Approach (MTA) developed by Deshmukh and Gadre (2009). As shown in Fig. 1b, each H-bond energy, E_{HB}, in ACE-$(Ala)_n$-NME is calculated by the following equation in the NFA:

$$E_{\mathrm{HB}} = E_{\mathrm{sys}} - E_{\mathrm{noA}} - E_{\mathrm{noD}} + E_{\mathrm{noAD}} \tag{1}$$

E_{sys}, E_{noA}, E_{noD}, and E_{noAD} represent the total electronic energy of the entire system, the system lacking the acceptor group, the system without the donor group, and the system lacking both the acceptor and donor groups, respectively.

In the NFA, we used the total electronic energy of the entire system $\left(E_{\mathrm{Total}}\right)$ as E_{sys} (Kondo et al. 2019, 2022), while the energy of the entire system was estimated using the energies of all fragments in the original MTA (Deshmukh and Gadre 2009). The total energies of the $\mathrm{WH_{alpha}}$-n models estimated by MTA $\left(E_{\mathrm{MTA}}\right)$ coincided well with the E_{Total} values of these models. The differences in the calculated values of E_{Total} and E_{MTA}, $E_{\mathrm{MTA}} - E_{\mathrm{Total}}$, were less than 0.09 kcal/mol. These differences are similar to that obtained in the previous study (Deshmukh and Gadre 2009) for the 3_{10}-helix (0.11 kcal/mol).

In addition to the H-bond energies, the NFA can approximately represent the change of electronic structures upon H-bond formation. The change in electron density upon H-bond formation, $\Delta\rho_{\mathrm{HB}}$, was evaluated as follows (Kondo et al. 2019, 2022):

$$\Delta\rho_{\mathrm{HB}} = \rho_{\mathrm{sys}} - \rho_{\mathrm{noA}} - \rho_{\mathrm{noD}} + \rho_{\mathrm{noAD}} \tag{2}$$

To examine the difference in the H-bond energy between the WH and MH models and between the ST and MH models in the context of their electronic structures, the differences in the change in electron density were computed using Eqs. 3 and 4, respectively:

$$\Delta\Delta\rho_{\mathrm{HB}}^{\mathrm{WH-MH}} = \Delta\rho_{\mathrm{HB}}^{\mathrm{WH}} - \Delta\rho_{\mathrm{HB}}^{\mathrm{MH}} \tag{3}$$

$$\Delta\Delta\rho_{\mathrm{HB}}^{\mathrm{ST-MH}} = \Delta\rho_{\mathrm{HB}}^{\mathrm{ST}} - \Delta\rho_{\mathrm{HB}}^{\mathrm{MH}} \tag{4}$$

As an advantage of NFA, no modifications of program code are required, though multiple calculations are needed. It indicates that we can utilize the NFA with any quantum chemical calculation programs.

For comparison and improvement of the force field, we also computed the H-bond energies based on the molecular mechanics (MM) with the AMBER ff99SB force field parameters (Wang et al. 2000), $E_{\mathrm{HB}}^{\mathrm{MM}}$, for the corresponding H-bonds as in the following equation:

$$E_{\mathrm{HB}}^{\mathrm{MM}} = \sum\nolimits_{i,j\in\{\mathrm{C,O,N,\ and\ H}\}} \frac{q_i q_j}{r_{ij}} + \sum\nolimits_{i,j\in\{\mathrm{C,O,N,\ and\ H}\}} \left(\frac{A_{ij}}{r_{ij}^{12}} - \frac{B_{ij}}{r_{ij}^{6}}\right) \tag{5}$$

where i and j are the atoms constituting the peptide group of an acceptor and a donor of an H-bond, respectively: {C, O, N, and H}. A_{ij} and B_{ij} are the Lennard–Jones coefficients, r_{ij} is the distance between atoms i and j, and q_i is the atomic partial charge of the atom i.

H-bond energies in helical model systems

In order to understand the effects of the helical secondary structures on the H-bond energies, we compared the H-bond energies for the $\mathrm{WH_{alpha}}$-n, $\mathrm{ST_{alpha}}$-n, and $\mathrm{MH_{alpha}}$-n models of α-helices and the $\mathrm{WH_{3\_10}}$-n, $\mathrm{ST_{3\_10}}$-n, and $\mathrm{MH_{3\_10}}$-n models of the 3_{10}-helices. Since the H-bond energies strongly depend on the spatial arrangement of the H-bond donor and acceptor atoms, we plotted the H-bond energies of the WH and ST models against those of the MH models for the α- and 3_{10}-helices in Fig. 2a and b, respectively, to cancel out the effect of the orientations of H-bond donor and acceptor (Kondo et al. 2022).

The H-bond energies obtained by the WH-n and ST-n models, $E_{\mathrm{HB}}^{\mathrm{WH}}$ and $E_{\mathrm{HB}}^{\mathrm{ST}}$, remarkably deviated from those calculated by the MH models. In the α-helices, the $\mathrm{ST_{alpha}}$-n model reproduced the H-bond energies of the $\mathrm{WH_{alpha}}$-n model. In contrast, the $\mathrm{MH_{alpha}}$-n model provided more stable H-bond energy than the $\mathrm{WH_{alpha}}$-n model (Fig. 2a), indicating that the adjacent residues covalently connecting the H-bond donor and acceptor destabilized the H-bond in the $\mathrm{WH_{alpha}}$-n model. In the 3_{10}-helices, the $\mathrm{ST_{3\_10}}$-n models also destabilized the H-bond as well as the α-helices compared to the $\mathrm{MH_{3\_10}}$-n models but failed to provide the

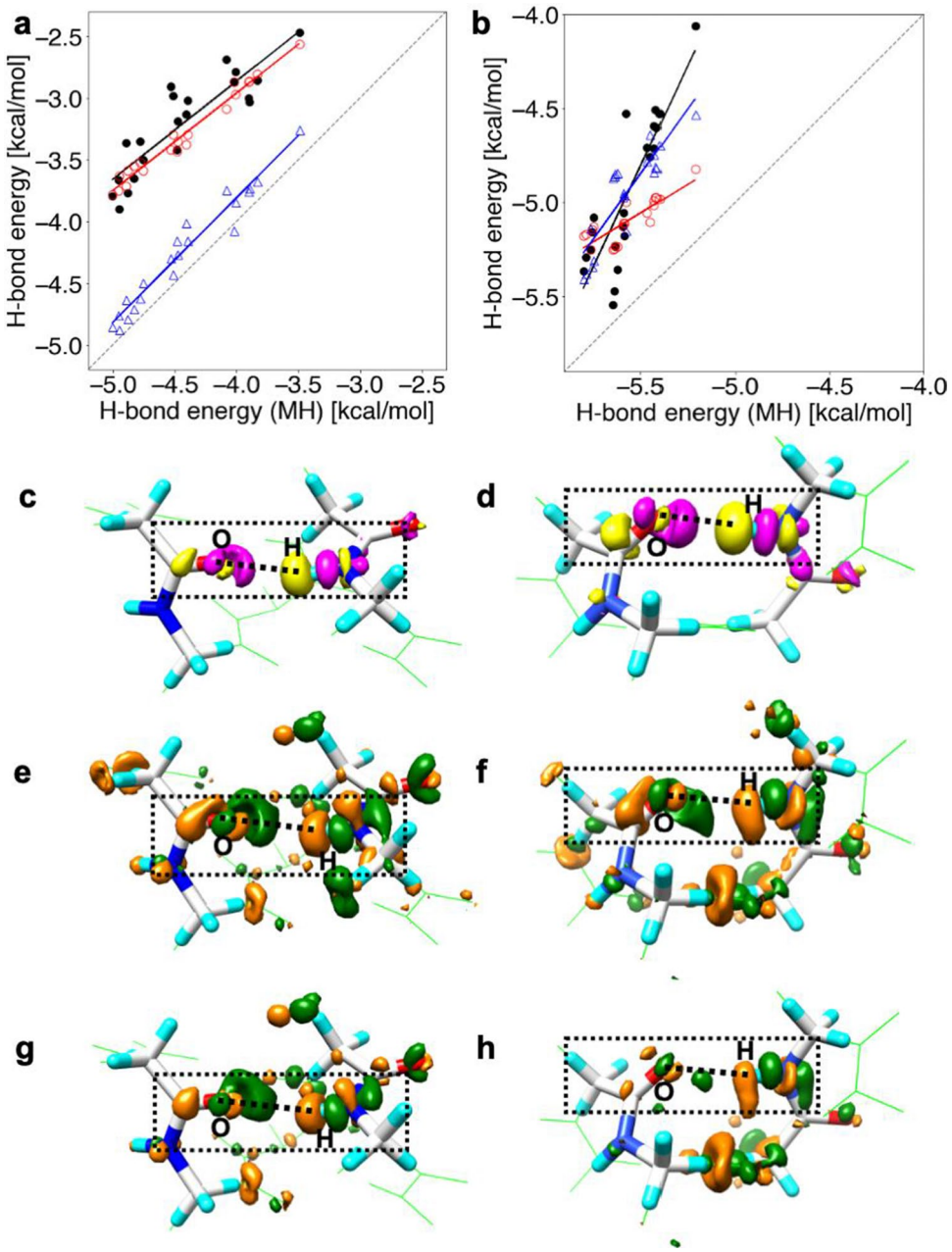

Fig. 2 Correlations of the H-bond energies of the WH (black filled circle), ST (red open circle), and MM (blue open triangle) models versus those of the MH model in **a** the α-helices and **b** the 3_{10}-helices. The dashed line shows a guide where the longitudinal axis values have identical H-bond energies (Kondo et al. 2022). Electron density changes upon H-bond formation, **c** $\Delta\rho_{HB}^{WH_{alpha}}$ and **d** $\Delta\rho_{HB}^{WH_{3\_10}}$, for 5-2 of the WH_{alpha}-5 model and for 4-2 of the WH_{3_10}-4 model. The yellow surfaces represent the contour surfaces at −0.001 au, and the magenta ones are those at +0.001 au. The atoms in the whole WH models are shown by green wire and those in the MH models are shown using the stick model with CPK colors. The difference in the change in electron density between the WH and ST models, $\Delta\Delta\rho_{HB}^{WH_{alpha}-MH_{alpha}}$ for **e** 5-2 of the WH_{alpha}-5 model and $\Delta\Delta\rho_{HB}^{WH_{3\_10}-MH_{3\_10}}$ for **f** 4-2 of the WH_{3_10}-4 model. The difference in the change in electron density between the ST and MH models, $\Delta\Delta\rho_{HB}^{ST_{alpha}-MH_{alpha}}$ for **g** 5-2 of the WH_{alpha}-5 model and $\Delta\Delta\rho_{HB}^{ST_{3\_10}-MH_{3\_10}}$ for **h** 4-2 of the WH_{3_10}-4 model. The dark-green surfaces are the contour surfaces at −0.00015 au, and the orange ones are those at +0.00015 au. The black dotted line is the H-bond between the oxygen atom of the C=O group at the *i*th residue and the hydrogen atom of the N-H group at the $(i + 4)$th residue. The corresponding hydrogen bond is surrounded by a dashed rectangle. Figures **d**, **f**, and **h** were slightly modified from the original figures, which appeared in the previous paper by Kondo et al. (2022)

equivalent H-bond energies of the WH_{3_10}-*n*. In particular, the H-bond pairs adjacent to the N- or C-terminal H-bond of the WH_{3_10}-*n* models were strongly destabilized compared to those of the ST_{3_10}-*n* models, resulting in the worse correlation of the WH_{3_10}-*n* and ST_{3_10}-*n* models. Details are discussed in our previous study (Kondo et al. 2022). It suggests

that the destabilization of the H-bond of the 3_{10}-helices is partly due to the helical backbone atoms linking the H-bond donor and acceptor. However, there should also be other factors leading to unstable H-bond energies.

We compared QM (E_{HB}^{WH}) and MM (E_{HB}^{MM}) calculations for the H-bond energies of the WH_{alpha}-*n* and WH_{3_10}-*n* models (Fig. 2a, b). In the WH_{alpha}-*n* models, the E_{HB}^{WH} values strongly correlated with the E_{HB}^{MM} values, but the MM calculations overestimated the stability of the H-bond energies by ~ 1 kcal/mol. The E_{HB}^{MM} values of the WH_{alpha}-*n* models almost coincided with the H-bond energies calculated by the MH models, E_{HB}^{MH}. This is because the current force field parameters of amino acids are adjusted based on the amino acid monomer. In contrast, the H-bond energies evaluated with the QM calculations were closer to those with the MM calculations for the WH_{3_10}-*n* models than for the WH_{alpha}-*n* models. However, the correlation between the QM and MM calculations was weak, unlike the WH_{alpha}-*n* models. In contrast to α-helices, the E_{HB}^{MH} values were more stable than the E_{HB}^{MH} values in 3_{10}-helices. This is because the H-bonds in the MH_{3_10}-*n* are much shorter than those in the MH_{alpha}-*n* models, thus having stronger quantum nature that the classical force field cannot describe.

Electronic structures around the H-bond donors and acceptors

The electron density changes for the WH_{alpha}-5 and WH_{3_10}-5 models, $\Delta\rho_{HB}^{WH_{alpha}}$ and $\Delta\rho_{HB}^{WH_{3\_10}}$, were calculated with Eq. 2 and are shown in Fig. 2c and d, respectively. Here, yellow and magenta colors show the negative and positive contour surfaces, respectively. From the $\Delta\rho_{HB}^{WH_{alpha}}$ values, the electron density increased around the oxygen atom of the C=O group at the *i*th residue and decreased around the hydrogen atom of the N–H group at the $(i+4)$th residue, as shown in Fig. 2c. The $\Delta\rho_{HB}^{WH_{3\_10}}$ values showed that the electron density increased in the vicinity of the oxygen atom of the C=O group at the *i*th residue and that it decreased in the vicinity of the hydrogen atom of the N–H group at the $(i+3)$th residue, as illustrated in Fig. 2d. The $\Delta\rho_{HB}^{WH_{alpha}}$ and $\Delta\rho_{HB}^{WH_{3\_10}}$, thus, implied the formation of the H-bond.

In Fig. 2e and g, the differences in electron density change between the WH_{alpha}-5 and MH_{alpha}-5 models and between the ST_{alpha}-5 and MH_{alpha}-5 models, $\Delta\Delta\rho_{HB}^{WH_{alpha}-MH_{alpha}}$ and $\Delta\Delta\rho_{HB}^{ST_{alpha}-MH_{alpha}}$, respectively, were shown for the α-helical turn 5-2. Here, green and orange colors show the negative and positive contour surfaces, respectively. The electron density changes near the oxygen atom of the C=O group at the *i*th residue in both the WH_{alpha} and ST_{alpha} models were smaller than that in the MH_{alpha} model, implying that the negative polarization of the oxygen atom was weakened by the backbone atoms linking the H-bond donor and acceptor. In contrast, the electron density near the hydrogen atom of the N–H group at the $(i+4)$th residue increased in the WH_{alpha} and ST_{alpha} models, as compared with that in the MH_{alpha} model. In addition, the $\Delta\Delta\rho_{HB}^{WH_{alpha}-MH_{alpha}}$ value was similar to the $\Delta\Delta\rho_{HB}^{ST_{alpha}-MH_{alpha}}$ values. It indicates that the weaker positive polarization of the hydrogen atom is mainly due to the adjacent residues connecting the H-bond donor and acceptor. We found that the distances between the oxygen atoms in the carbonyl group of the *i*th and $(i+1)$th residues in the H-bond pairs were short (3.510 ± 0.144 Å). In addition, those between the hydrogen atoms in the amide group of the $(i+3)$th and $(i+4)$th residues were also short (2.676 ± 0.038 Å). These short distances caused the depolarization of both the carbonyl oxygen of the *i*th residue and the amide hydrogen of the $(i+4)$th residue, as revealed in Fig. 2e and g. The depolarized electronic structures around the carbonyl oxygen of the *i*th residue and the amide hydrogen of the $(i+4)$th residue generally resulted in weaker H-bond energies for the α-helix, as in the WH_{alpha} and ST_{alpha} models, than for the separated H-bonds, as in the MH_{alpha} model. Such depolarizations redistributing the electron density were caused by the local electronic interactions in their neighborhood inside the α-helical structure.

Figure 2f and h show $\Delta\Delta\rho_{HB}^{WH_{3\_10}-MH_{3\_10}}$ and $\Delta\Delta\rho_{HB}^{ST_{3\_10}-MH_{3\_10}}$ values for the 3_{10}-helical turn 4–2. The $\Delta\Delta\rho_{HB}^{WH_{3\_10}-MH_{3\_10}}$ and $\Delta\Delta\rho_{HB}^{ST_{3\_10}-MH_{3\_10}}$ values indicated depolarization of the oxygen atom of the C=O group at the *i*th residue and the hydrogen atom of the N–H group at the $(i+3)$th residue in the WH_{3_10} and ST_{3_10} models. However, in contrast to the $\Delta\Delta\rho_{HB}^{WH_{alpha}-MH_{alpha}}$ and $\Delta\Delta\rho_{HB}^{ST_{alpha}-MH_{alpha}}$ values, the $\Delta\Delta\rho_{HB}^{WH_{3\_10}-MH_{3\_10}}$ values for the 3_{10}-helical turn 4–2 were remarkably different from the $\Delta\Delta\rho_{HB}^{ST_{3\_10}-MH_{3\_10}}$ values, implying other factors besides the helical backbone atoms linking the H-bond pairs that caused the depolarization of the H-bond donor and acceptor in the 4–2 pair. We now discuss why the H-bonds in the ST_{3_10}-*n* model were destabilized in comparison to those in the MH_{3_10}-*n* model. We found that the C=O group at the *i*th residue and the N–H group at the $(i+3)$th residue of the H-bond were depolarized in the ST_{3_10}-*n* model, as shown in Fig. 2h. This depolarization could be caused by the helical backbone atoms linking the H-bond pair. Whereas the C=O group at the $(i+1)$th residue was involved in depolarization in α-helices, the C=O group of the H-bond pair was closer to the adjacent N–H group at the $(i+2)$th residue (2.799 ± 0.033 Å), than to the adjacent C=O group at the $(i+1)$th residue (3.442 ± 0.025 Å) in the 3_{10}-helices. Therefore, in the 3_{10}-helices, the adjacent N–H group may cause the depolarization of the H-bond acceptor, resulting in only little destabilization of the H-bond.

Toward improvement of the H-bond energy by the classical force field

Our calculations for α-helices and 3_{10}-helices with the NFA revealed that their H-bond energies are affected by depolarization and polarization due to the local dipole of the neighboring backbone peptide groups. Based on our results, we constructed a model for the classical force field, in which the atomic partial charges (q_N^i, q_H^i, q_C^i, and q_O^i) of the N–H and C=O groups of the ith peptide group were not constant but were changed by the neighboring peptide groups, respectively.

$$q_N^i = q_N^0\left(1-\delta_N^i\right) \tag{6}$$

$$q_H^i = q_H^0\left(1-\delta_H^i\right) \tag{7}$$

$$q_C^i = q_C^0\left(1-\delta_C^i\right) \tag{8}$$

$$q_O^i = q_O^0\left(1-\delta_O^i\right) \tag{9}$$

where q_N^0, q_H^0, q_C^0, and q_O^0 are the original atomic partial charge, and the amounts of changes in the atomic partial charges of the ith peptide group; δ_N^i, δ_H^i, δ_C^i, and δ_O^i, are functions depending on the backbone structure of the neighboring peptide group. This change may be represented by the interaction energy of the classical mechanics, $U\left(\vec{\mu}_X^i, \vec{\mu}_Y^j\right)$ between the ith backbone dipole, $\vec{\mu}_X^i$ (X = NH or CO), and the neighboring backbone dipole, $\vec{\mu}_Y^j$ (Y = NH or CO) ($j \neq i$). To avoid double counting interaction energies already taken in contributions in the restrained electrostatic potential (RESP) approach (Bayly et al. 1993; Cieplak et al. 1995), the following formula was used to obtain the change in the original atomic partial charge.

$$\delta_H^i = \lambda_{HO}\left[U\left(\vec{\mu}_{NH}^i, \vec{\mu}_{CO}^{i-1}\right)\right] + \lambda_{HH}\left[U\left(\vec{\mu}_{NH}^i, \vec{\mu}_{NH}^{i-1}\right)\right] \tag{10}$$

$$\delta_O^i = \lambda_{OO}\left[U\left(\vec{\mu}_{CO}^i, \vec{\mu}_{CO}^{i+1}\right)\right] + \lambda_{OH}\left[U\left(\vec{\mu}_{CO}^i, \vec{\mu}_{NH}^{i+1}\right)\right] \tag{11}$$

where λ_{HO}, λ_{HH}, λ_{OO}, and λ_{OH} are fitting parameters. To ensure that the overall charge does not change, local neutrality conditions were imposed, and δ_N^i and δ_C^i are defined as follows.

$$\delta_N^i q_N^0 = -\delta_H^i q_H^0 \tag{12}$$

$$\delta_C^i q_C^0 = -\delta_O^i q_O^0 \tag{13}$$

We determined the parameters λ_{HO}, λ_{HH}, λ_{OO}, and λ_{OH}, by using the H-bond energies calculated with NFA, E_{HB}^{WH}, for both α-helices and 3_{10}-helices, and those of the AMBER ff99SB force field parameters (Wang et al. 2000), E_{HB}^{MM}. Using the determined fitting parameters, we modified the MM values of the H-bond energies, denoted as $E_{HB}^{MM_{modified}}$, and plotted the $E_{HB}^{MM_{modified}}$ versus E_{HB}^{WH} (open symbols), together with the original E_{HB}^{MM}

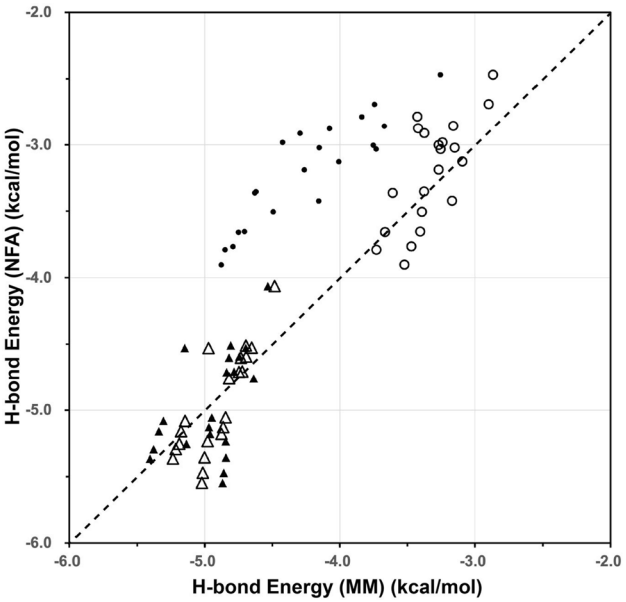

Fig. 3 Correlations of the $E_{HB}^{MM_{modified}}$ and E_{HB}^{WH} (open symbols), together with those of the E_{HB}^{MM} and E_{HB}^{WH} (small filled symbols) for both in the α-helices (circles) and the 3_{10}-helices (triangles). The dashed line shows a guide where the longitudinal axis values from NFA have the identical H-bond energies by the MM and $MM_{modified}$ methods. The detail of the latter modification is as follows: the modified H-bond energy $E_{HB}^{MM_{modified}} = \sum_{ij}\frac{q_i q_j}{r_{ij}} + \sum_{ij}\left(\frac{A_{ij}}{r_{ij}^{12}} - \frac{B_{ij}}{r_{ij}^{6}}\right)$ was computed from the modified charges, q_N, q_H, q_C, and q_O, given by Eqs. (6)–(9) as the changes from the original charges, q_N^0, q_H^0, q_C^0, and q_O^0, which were −0.4157, 0.2719, 0.5973, and −0.5679, respectively, taken from the AMBER ff99SB force field (Wang et al. 2000). The parameters modifying charges, δ_N^i, δ_H^i, δ_C^i, and δ_O^i, in Eqs. (6)–(9) were computed by Eqs. (10)–(13), where the fitting parameters λ_{HO}, λ_{HH}, λ_{OO}, and λ_{OH} were the coefficients of the interaction energies between the ith backbone dipole, $\vec{\mu}_X^i$ (X = HN or CO), and the neighboring backbone dipole, $\vec{\mu}_Y^j$ (Y = HN or CO) ($j \neq i$), as in Eqs. (10) and (11): $U\left(\vec{\mu}_X^i, \vec{\mu}_Y^j\right) = \frac{\vec{\mu}_X^i \vec{\mu}_Y^j}{r_{ij}^3} - \frac{3\left(\vec{\mu}_X^i \vec{r}_{ij}\right)\left(\vec{\mu}_Y^j \vec{r}_{ij}\right)}{r_{ij}^5}$. Here, r_{ij} is the distance between the center of the ith backbone dipole and that of the jth dipole. The local dipole moments were given as $\vec{\mu}_{CO}^k = \frac{1}{2}\left(q_C^k - q_O^k\right)\left(\vec{r}_C^k - \vec{r}_O^k\right)$ and $\vec{\mu}_{HN}^k = \frac{1}{2}\left(q_H^k - q_N^k\right)\left(\vec{r}_H^k - \vec{r}_N^k\right)$ (k = i or j), as indicated in Kondo et al. (2019). The four parameters λ_{HO}, λ_{HH}, λ_{OO}, and λ_{OH} were determined by minimizing the square of the difference between $E_{HB}^{MM_{modified}}$ and E_{HB}^{WH} simultaneously for H-bond energies of 21 WH_{alpha} values of α-helices (Kondo et al. 2019) and for those of 21 WH_{3_10} values of 3_{10}-helices (Kondo et al. 2022). The resulted parameters were λ_{HO} = −11.535, λ_{HH} = 38.517, λ_{OO} = 16.967, and λ_{OO} = 4.587, respectively, where the unit was all (kcal/mol)

versus E_{HB}^{WH} (small filled symbols) in Fig. 3. The root mean square deviation of the original E_{HB}^{MM} from the E_{HB}^{WH} values was evaluated to be 0.78 kcal/mol, and that of the $E_{HB}^{MM_{modified}}$ from the E_{HB}^{WH} values was calculated to be 0.28 kcal/mol, much smaller than the original one. It suggests that this modification of the classical MM force field could well approximate the H-bond energies provided by NFA. In particular, those for the α-helices were remarkably improved, as shown in Fig. 3. For extended structures, the amounts of changes in the atomic partial charges should be small because the dipole–dipole interaction quickly decreases in inverse proportion of the cube of the distance between the dipole pair.

Concluding remarks

We have briefly reviewed our recent computational studies of hydrogen bonds (H-bonds) in helical secondary structures of proteins, α-helix and 3_{10}-helix, using a Negative Fragmentation Approach (NFA) with density functional theory (DFT). Our computation showed that the H-bond energies of the α-helix are generally weaker than those of the separated H-bonds due to the depolarized electronic structures around the carbonyl oxygen of the ith residue and the amide hydrogen of the $(i+4)$th residue. The H-bond energies of the 3_{10}-helix are also weaker than those of the separated H-bonds, but the effects are not so large as those for the α-helix. Whereas the adjacent C=O group is involved in the depolarization of the H-bond acceptor in α-helices, the C=O group of the H-bond pair is closer to the adjacent N–H group than to the adjacent C=O group in the 3_{10}-helices. Therefore, the weak destabilization of the H-bond is attributed to the balance of the depolarization and polarization caused by the adjacent N–H group and the C=O group. Based on the findings from our computational results, a model was constructed in which the atomic partial charges of the N–H and C=O groups of the backbone peptide groups forming H-bonds are changed by the neighboring peptide groups, respectively. This modified MM model well reproduced the H-bond energies of α-helices and 3_{10}-helices given by the NFA computation. We expect that this modification could lead to more reliable MD simulations in the future.

Supplementary Information The online version contains supplementary material available at https://doi.org/10.1007/s12551-022-01034-5.

Acknowledgements The computations were performed at the Research Center for Computational Science, Okazaki, Japan (22-IMS-C007), and the RIKEN Advanced Center for Computing and Communication (ACCC). This study was performed in part under the Cooperative Research Program of the Institute for Protein Research, Osaka University, CR-21-02 and CR-22-02.

Author contribution Yu Takano and Haruki Nakamura contributed to the study conception and design. Data collection and analysis were performed by Hiroko X. Kondo, Haruki Nakamura, and Yu Takano. The first draft of the manuscript was written by Yu Takano and Hiroko X. Kondo, and all authors commented on previous versions of the manuscript. All authors read and approved the final manuscript.

Funding This study was funded by the Japan Society for the Promotion of Science (JSPS) for Grants-in-Aid for Scientific Research (C) (19K06589 and 22K06164) and the Ministry of Education, Culture, Sports, Science and Technology (MEXT) for a Grant-in-Aid for Scientific Research on Transformative Research Areas (A) "Hyper-Ordered Structures Science" (20H05883).

Data availability The data that support the findings of this study are available from the corresponding author upon reasonable request.

Declarations

Ethical approval This article does not contain any studies with animals performed by any of the authors.

Conflict of interest The authors declare no competing interests.

References

Arnott S, Dover SD (1967) Refinement of bond angles of an α-helix. J Mol Biol 30:209–212. https://doi.org/10.1016/0022-2836(67)90253-7

Barlow DJ, Thornton JM (1988) Helix geometry in proteins. J Mol Biol 201:601–619. https://doi.org/10.1016/0022-2836(88)90641-9

Bayly CI, Cieplak P, Cornell W, Kollman PA (1993) A well-behaved electrostatic potential based method using charge restraints for deriving atomic charges: the RESP model. J Phys Chem 97:10269–10280. https://doi.org/10.1021/j100142a004

Best RB, Hummer G (2009) Optimized molecular dynamics force fields applied to the helix−coil transition of polypeptides. J Phys Chem B 113:9004–9015. https://doi.org/10.1021/jp901540t

Best RB, Buchete N-V, Hummer G (2008) Are current molecular dynamics force fields too helical? Biophys J 95:L07–L09. https://doi.org/10.1529/biophysj.108.132696

Branden CI, Tooze J (2012) Introduction to protein Structure, 2nd Edition. Garland Science, New York Science. https://doi.org/10.1201/9781136969898

Buck M, Bouguet-Bonnet S, Pastor RW, MacKerell AD (2006) Importance of the CMAP correction to the CHARMM22 protein force

field: dynamics of hen lysozyme. Biophys J 90:L36–L38. https://doi.org/10.1529/biophysj.105.078154
Chebaro Y, Ballard AJ, Chakraborty D, Wales DJ (2015) Intrinsically Disordered Energy Landscapes. Sci Rep 5:10386. https://doi.org/10.1038/srep10386
Cieplak P, Cornell WD, Bayly C, Kollman PA (1995) Application of the multimolecule and multiconformational RESP methodology to biopolymers: Charge derivation for DNA, RNA, and proteins. J Comput Chem 16:1357–1377. https://doi.org/10.1002/jcc.540161106
Cornell WD, Cieplak P, Bayly CI et al (1995) A second generation force field for the simulation of proteins, nucleic acids, and organic molecules. J Am Chem Soc 117:5179–5197. https://doi.org/10.1021/ja00124a002
Deshmukh MM, Gadre SR (2009) Estimation of N−H···O═C intramolecular hydrogen bond energy in polypeptides. J Phys Chem A 113:7927–7932. https://doi.org/10.1021/jp9031207
Eisenberg D (2003) The discovery of the α-helix and β-sheet the principal structural features of proteins. Proc Natl Acad Sci USA 100:11207–11210. https://doi.org/10.1073/pnas.2034522100
Fujitani H, Matsuura A, Sakai S et al (2009) High-level ab initio calculations to improve protein backbone dihedral parameters. J Chem Theory Comput 5:1155–1165. https://doi.org/10.1021/ct8005437
Grimme S (2006) Semiempirical GGA-type density functional constructed with a long-range dispersion correction. J Comput Chem 27:1787–1799. https://doi.org/10.1002/jcc.20495
Head-Gordon M, Pople JA, Frisch MJ (1988) MP2 energy evaluation by direct methods. Chem Phys Lett 153:503–506. https://doi.org/10.1016/0009-2614(88)85250-3
Higo J, Nishimura Y, Nakamura H (2011) A free-energy landscape for coupled folding and binding of an intrinsically disordered protein in explicit solvent from detailed all-atom computations. J Am Chem Soc 133:10448–10458. https://doi.org/10.1021/ja110338e
Holde Van KE, Johnson WC, Ho PS (1998) Principles of physical biochemistry. Prentice-Hall Inc., New Jersey
Ismer L, Ireta J, Neugebauer J (2008) First-principles free-energy analysis of helix stability: the origin of the low entropy in π helices. J Phys Chem B 112:4109–4112. https://doi.org/10.1021/jp077728n
Kamiya N, Watanabe YS, Ono S, Higo J (2005) AMBER-based hybrid force field for conformational sampling of polypeptides. Chem Phys Lett 401:312–317. https://doi.org/10.1016/j.cplett.2004.11.070
Kollman P, Dixon R, Cornell W et al (1997) The development/application of a 'minimalist' organic/biochemical molecular mechanic force field using a combination of ab initio calculations and experimental data. In: Computer Simulation of Biomolecular Systems. Springer Netherlands, Dordrecht, pp 83–96
Kondo HX, Kusaka A, Kitakawa CK et al (2019) Hydrogen bond donors and acceptors are generally depolarized in α-helices as revealed by a molecular tailoring approach. J Comput Chem 40:2043–2052. https://doi.org/10.1002/jcc.25859
Kondo HX, Nakamura H, Takano Y (2022) Depolarizing effects in hydrogen bond energy in 310-helices revealed by quantum chemical analysis. Int J Mol Sci 23:9032. https://doi.org/10.3390/ijms23169032
Kuster DJ, Liu C, Fang Z et al (2015) High-resolution crystal structures of protein helices reconciled with three-centered hydrogen bonds and multipole electrostatics. PLoS One 10:e0123146. https://doi.org/10.1371/journal.pone.0123146
Liljas A, Liljas L, Ash M-R et al (2017) Textbook of structural biology, 2nd Edition. World Scientific Publishing, Singapore. https://doi.org/10.1142/10102
Lopes PEM, Roux B, MacKerell AD (2009) Molecular modeling and dynamics studies with explicit inclusion of electronic polarizability: theory and applications. Theor Chem Acc 124:11–28. https://doi.org/10.1007/s00214-009-0617-x
Morozov AV, Tsemekhman K, Baker D (2006) Electron density redistribution accounts for half the cooperativity of α helix formation. J Phys Chem B 110:4503–4505. https://doi.org/10.1021/jp057161f
Nishigami H, Kamiya N, Nakamura H (2016) Revisiting antibody modeling assessment for CDR-H3 loop. Protein Eng Des Sel 29:477–484. https://doi.org/10.1093/protein/gzw028
Parthasarathi R, Raman SS, Subramanian V, Ramasami T (2007) Bader's electron density analysis of hydrogen bonding in secondary structural elements of protein. J Phys Chem A 111:7141–7148. https://doi.org/10.1021/jp071513w
Patel S, Brooks CL (2004) CHARMM fluctuating charge force field for proteins: I parameterization and application to bulk organic liquid simulations. J Comput Chem 25:1–16. https://doi.org/10.1002/jcc.10355
Pauling L, Corey RB, Branson HR (1951) The structure of proteins: two hydrogen-bonded helical configurations of the polypeptide chain. Proc Natl Acad Sci USA 37:205–211. https://doi.org/10.1073/pnas.37.4.205
Petsko GA, Ringe D (2004) Protein structure and function. New Science Press, London
Piana S, Lindorff-Larsen K, Shaw DE (2011) How robust are protein folding simulations with respect to force field parameterization? Biophys J 100:L47–L49. https://doi.org/10.1016/j.bpj.2011.03.051
Robustelli P, Piana S, Shaw DE (2018) Developing a molecular dynamics force field for both folded and disordered protein states. Proc Natl Acad Sci 115:E4758–E4766. https://doi.org/10.1073/pnas.1800690115
Sakae Y, Okamoto Y (2003) Optimization of protein force-field parameters with the Protein Data Bank. Chem Phys Lett 382:626–636. https://doi.org/10.1016/j.cplett.2003.10.107
Saleh G, Gatti C, Lo Presti L, Contreras-García J (2012) Revealing non-covalent interactions in molecular crystals through their experimental electron densities. Chem - A Eur J 18:15523–15536. https://doi.org/10.1002/chem.201201290
Scuseria GE, Schaefer HF (1989) Is coupled cluster singles and doubles (CCSD) more computationally intensive than quadratic configuration interaction (QCISD)? J Chem Phys 90:3700–3703. https://doi.org/10.1063/1.455827
Shirai H, Ikeda K, Yamashita K et al (2014) High-resolution modeling of antibody structures by a combination of bioinformatics, expert knowledge, and molecular simulations. Proteins Struct Funct Bioinforma 82:1624–1635. https://doi.org/10.1002/prot.24591
Takano Y, Yonezawa Y, Fujita Y et al (2011) Electronic structures of a [4Fe–4S] cluster, [Fe4S4(SCH3)3(CH3COO)], in dark-operative protochlorophyllide oxidoreductase (DPOR). Chem Phys Lett 503:296–300. https://doi.org/10.1016/j.cplett.2011.01.026
Takano Y, Shigeta Y, Koizumi K, Nakamura H (2012) Electronic structures of the Cu2S2 core of the CuA site in cytochrome c oxidase and nitrous oxide reductase. Int J Quantum Chem 112:208–218. https://doi.org/10.1002/qua.23191
Takano Y, Kusaka A, Nakamura H (2016) Density functional study of molecular interactions in secondary structures of proteins. Biophys Physicobiology 13:27–35. https://doi.org/10.2142/biophysico.13.0_27
Tantardini C (2019) When does a hydrogen bond become a van der Waals interaction? a topological answer. J Comput Chem 40:937–943. https://doi.org/10.1002/jcc.25774
Tantardini C, Michalchuk AAL, Samtsevich A et al (2020) The Volumetric source function: looking inside van der Waals interactions. Sci Rep 10:7816. https://doi.org/10.1038/s41598-020-64261-4
Wang J, Cieplak P, Kollman PA (2000) How well does a restrained electrostatic potential (RESP) model perform in calculating conformational energies of organic and biological molecules?

J Comput Chem 21:1049–1074. https://doi.org/10.1002/1096-987X(200009)21:12%3c1049::AID-JCC3%3e3.0.CO;2-F

Wieczorek R, Dannenberg JJ (2003) H-bonding cooperativity and energetics of α-helix formation of five 17-amino acid peptides. J Am Chem Soc 125:8124–8129. https://doi.org/10.1021/ja035302q

Wieczorek R, Dannenberg JJ (2003) Hydrogen-bond cooperativity, vibrational coupling, and dependence of helix stability on changes in amino acid sequence in small 3 10 -helical peptides. a density functional theory study. J Am Chem Soc 125:14065–14071. https://doi.org/10.1021/ja034034t

Wu Y-D, Zhao Y-L (2001) A theoretical study on the origin of cooperativity in the formation of 3 10 - and α-helices. J Am Chem Soc 123:5313–5319. https://doi.org/10.1021/ja003482n

Yoda T, Sugita Y, Okamoto Y (2004) Comparisons of force fields for proteins by generalized-ensemble simulations. Chem Phys Lett 386:460–467. https://doi.org/10.1016/j.cplett.2004.01.078

Yoda T, Sugita Y, Okamoto Y (2004) Secondary-structure preferences of force fields for proteins evaluated by generalized-ensemble simulations. Chem Phys 307:269–283. https://doi.org/10.1016/j.chemphys.2004.08.002